Applied Catalysis B: Environmental 91 (2009) 157–164

Contents lists available at ScienceDirect

Applied Catalysis B: Environmental

journal homepage: www.elsevier.com/locate/apcatb

Highly enhanced photocatalytic degradation of tetramethylammonium on the hybrid catalyst of titania and MCM-41 obtained from rice husk silica

Surachai Artkla [a,c], Wooyul Kim [c], Wonyong Choi [c,**], Jatuporn Wittayakun [a,b,*]

[a] Material Chemistry Research Unit, School of Chemistry, Institute of Science, Suranaree University of Technology, Nakhon Ratchasima 30000, Thailand
[b] National Center of Excellence for Environmental and Hazardous Waste Management, Thammasat University, Pathumtani 12120, Thailand
[c] School of Environmental Science and Engineering, Pohang University of Science and Technology, Pohang 790-784, South Korea

ARTICLE INFO

Article history:
Received 27 February 2009
Received in revised form 12 May 2009
Accepted 13 May 2009
Available online 20 May 2009

Keywords:
Photocatalytic water treatment
Supported photocatalyst
TiO_2
Rice husk silica
MCM-41
Tetramethylammonium

ABSTRACT

A hybrid photocatalyst consisting of TiO_2 and the mesoporous support was prepared by loading TiO_2 nanoparticles on MCM-41 which was synthesized from silica obtained from rice husk (abundant agricultural waste in Thailand). The catalysts with varying content of TiO_2 were characterized by X-ray diffraction (XRD), nitrogen adsorption–desorption, high-resolution transmission electron microscopy (HRTEM), energy-dispersive X-ray (EDX) analysis and UV–vis diffuse reflectance spectroscopy. The MCM-41 structure was retained after the loading of TiO_2 but its surface area decreased as a result of the partial pore blocking. The TiO_2 morphology and band gap were not affected by the dispersion on the support but the presence of the support prevented the TiO_2 nanoparticles from agglomerating in the neutral pH range. When the TiO_2 loading on the support was higher than 10 wt.%, the activity of the hybrid catalyst was saturated. The activity of TiO_2/MCM-41 for the photocatalytic degradation of tetramethylammonium (TMA) in aqueous slurry was significantly higher than that of the unsupported TiO_2. The optimal TiO_2 loading on the support was 10 wt.% at which the complete conversion of TMA was achieved in 90 min irradiation at pH 7. The unsupported TiO_2 photocatalyst could convert only 20% of TMA in the same irradiation time and condition. The photocatalytic degradation of TMA proceeded by generating demethylated intermediates such as tri-, di- and monomethylammonium ions which were finally converted to ammonium ions.

1. Introduction

Tetramethylammonium hydroxide ($N(CH_3)_4OH$, TMAH) is a chemical that is widely used as a silicon etchant in semiconductor industry. Because of its recalcitrant and non-adsorbing nature, TMA is difficult to remove from contaminated water by conventional biological and physical methods [1–3]. The exposure to TMAH may irritate skin, eyes and respiratory tracts. Advanced oxidation processes (AOPs) that involve the generation of very reactive oxygen species such as hydroxyl radical ($HO^{\bullet}$) have been investigated to destruct this pollutant [4–8].

TiO_2/UV process is one of the promising AOPs that generates OH radicals on the illuminated surface of TiO_2 photocatalysts. The photocatalytic degradation (PCD) of TMA in water on TiO_2 was successfully carried out and reported to be highly dependent on pH and the electrostatic interation between TMA and TiO_2 surface [1]. The PCD was highly effective in alkaline solution because the electrostatic attraction between TMA cations and the negatively charged TiO_2 surface was dominant at high pH. However, when the pH was close to the point of zero charge (pH_{PZC} = 6.7) of bare TiO_2, the PCD activity of TMA was drastically hindered because the TiO_2 particles aggregated resulting in a decrease of surface area and the electrostatic attraction. Although the electrostatic repulsion between TMA and TiO_2 prevails at acidic pH, the PCD activity was higher than at neutral pH because the TiO_2 particles were better dispersed. Therefore, achieving a good dispersiveness of TiO_2 particles is very critical in obtaining higher photocatalytic activity for TMA degradation.

Several approaches have been carried out to modify the electrostatic and surface characteristics of the TiO_2 photocatalysts. Vohra et al. [9] coupled TiO_2 particles with SiO_2 (with lower pH_{PZC}) to modify the surface charge of titania and highly enhanced the PCD of TMA. A complete conversion of TMA was achieved in 2 h with SiO_2–TiO_2 whereas less than 80% conversion was obtained even after 6 h with bare TiO_2 (at pH 5). There were also reports on the composites between TiO_2 and mesoporous material such as MCM-41. Bouazza

* Corresponding author at: Material Chemistry Research Unit, School of Chemistry, Institute of Science, Suranaree University of Technology, 111 University Ave., Muang, Nakhon Ratchasima 30000, Thailand. Tel.: +66 44 224 256; fax: +66 44 224 185.
** Co-corresponding author. Tel.: +82 54 279 2283; fax: +82 54 279 8299.
E-mail addresses: wchoi@postech.edu (W. Choi), jatuporn@sut.ac.th (J. Wittayakun).

0926-3373/$ – see front matter © 2009 Elsevier B.V. All rights reserved.
doi:10.1016/j.apcatb.2009.05.019

et al. [10] made the photocatalyst pellets containing TiO_2 and MCM-41 (with 7:3 weight ratio) and observed that its photocatalytic activity for the oxidation of propene was higher than that of TiO_2 pellets. Phanikrishna Sharma et al. also prepared a composite of TiO_2/Al-MCM-41 by solid state dispersion method and demonstrated its PCD activity for isoproturon herbicide under solar light [11].

In this work we synthesized a hybrid photocatalyst that consisted of TiO_2 nanoparticles dispersed on RH-MCM-41, a mesoporous material synthesized from rice husk silica. RH-MCM-41 has a high specific surface area (up to 1231 m^2/g) as a catalyst support and could be obtained from a recycled product of agricultural wastes [12–17]. The dispersion of TiO_2 nanoparticles on MCM-41 support is expected to prevent their agglomeration by maintaining the photocatalytic activity of the nanoparticles. In addition, the acidic silicic framework of RH-MCM-41 provides the environment of the negative surface charge on the hybrid catalyst which is highly favorable for the degradation of TMA cations over a wide range of pH. Therefore, the PCD of TMA with the present hybrid photocatalyst can be more efficiently carried out in the neutral pH region where PCD with bare TiO_2 was minimal because of the catalyst agglomeration. The TiO_2/RH-MCM-41 was characterized by using various analytical methods and its photocatalytic activity for TMA degradation was investigated in detail.

2. Experimental and methods

2.1. Chemicals

2.1.1. Reagents for RH-MCM-41 and TiO_2/RH-MCM-41 synthesis

Rice husk silica was prepared by acid leaching as described by Wittayakun et al. [18]. The following reagent-grade chemicals were used as received: cetyltrimethylammonium bromide or CTAB (96% $C_{19}H_{42}BrN$, Fluka), sodium hydroxide (97% NaOH, Carlo Erba), sulfuric acid (96% H_2SO_4, Carlo Erba) and titanium dioxide (TiO_2 Degussa P25).

2.1.2. Chemicals for photocatalytic degradation of TMA

The following chemicals were used for photodegradation of TMA as received: $(CH_3)_4NCl$ (ACROS Organics), $(CH_3)_3NHCl$ (Aldrich), $(CH_3)_2NH_2Cl$ (Sigma), CH_3NH_3Cl (Sigma), NH_4Cl (Aldrich), $(C_2H_5)_4NCl$ (Sigma), methanesulfonic acid (Aldrich), Na_2CO_3 (S.P.C. GR Reagent, Japan), $NaHCO_3$ (Kanto, Japan), CH_3CN (Aldrich), HCl (S.P.C. GR Reagent, Japan), and LiOH (S.P.C. GR Reagent, Japan). A Barnstead water purification setup was employed to obtain the deionized water (18 Ω).

2.2. Preparation of RH-MCM-41and TiO_2/RH-MCM-41

Rice husk silica was prepared by acid leaching as described by Wittayakun et al. [18] and used as a silica source for the synthesis of RH-MCM-41. A solution of CTAB was mixed with sodium silicate prepared from rice husk silica in 3.33 mol/L NaOH solution to produce a gel with the molar ratio of 1.0SiO_2:3.0NaOH:0.25CTAB:180H_2O. The mixture pH was adjusted to 11.5 and the gel was crystallized at 100 °C for 24 h, filtered, dried, and calcined at 540 °C for 6 h [19].

The TiO_2/RH-MCM-41 was prepared by adding a desired amount of TiO_2 (Degussa P25) to a slurry of RH-MCM-14 in deionized water under continuous stirring for 2 h. The mixture was washed several times with deionized water to remove Na^+ ions, dried and calcined at 300 °C for 6 h. The prepared TiO_2/RH-MCM-41 catalysts contained 10, 20, 40 or 60 wt.% of TiO_2.

2.3. Catalyst characterization

The crystalline phase of bare TiO_2 and TiO_2/RH-MCM-41 was analyzed using powder X-ray diffraction (XRD: Rigaku Model D/Max III) with CuK_α radiation. The catalyst powder (0.20 g) was pressed in a sample holder and scanned from 10° to 80° (2θ) in steps of 0.05°/min. The diffraction patterns of the various powder samples were recorded with the same mass of the sample so that the diffraction intensity could be compared among different samples. The high-resolution transmission electron micrographs (HRTEM) and energy-dispersive X-ray (EDX) analysis of bare TiO_2, RH-MCM-41 and TiO_2/RH-MCM-41 powders were obtained using a JEM-2100F microscope with Cs-corrected.

The UV absorption spectra of bare TiO_2, RH-MCM-41 and TiO_2/RH-MCM-41 powders were recorded using a Shimadzu UV–vis spectrophotometer equipped with a diffuse reflectance attachment (Shimadzu ISR-2200). All sample powders were diluted with $BaSO_4$ (TiO_2:$BaSO_4$ = 1:17) and their diffuse reflectance were referenced against $BaSO_4$.

To characterize the surface charge properties of RH-MCM-41 and TiO_2/RH-MCM-41, the electrokinetic potential or zeta potential of the suspended catalyst particles was measured. The electrophoretic mobilities of bare TiO_2, RH-MCM-41 and TiO_2/RH-MCM-41 particles were measured in aqueous suspension (0.5 g/L) to determine their zeta potentials as a function of pH by using an electrophoretic light scattering spectrophotometer (ELS 8000, Otsuka) equipped with a He–Ne laser and a thermostated flat board cell.

Surface area and pore structure of the sample were determined by N_2 adsorption–desorption isotherm at liquid nitrogen temperature in the relative pressure ranging from 0.01 to 0.99 with a Micromeritics ASAP 2010 (Autosorb-1 series). Before the measurement, each sample was degassed at 250 °C for 3 h in vacuum. The BET surface area was obtained from the N_2 adsorption data in the relative pressure range of 0.02–0.2. The pore diameter was calculated from the desorption branches according to Barrett–Joyner–Halenda (BJH) method.

2.4. Photocatalytic degradation of TMA

All experiments were carried out in a pyrex reactor (33 mL) with a quartz window. A Xe-arc lamp (300 W, Oriel) was used as the light source. All bare TiO_2 and TiO_2/RH-MCM-41 suspensions were prepared at a concentration of 0.1 and 1 g/L, respectively and dispersed by simultaneous sonication and shaking for 30 s. An aliquot of TMA stock solution (1 mM) was subsequently added to the suspension to give a desired concentration. The initial pH of the suspension (pH_i) was adjusted with HCl or LiOH standard solutions. The suspension was subsequently irradiated by UV light ($\lambda > 300$ nm) and the sample aliquots of 1 mL were collected at appropriate time intervals and filtered through 0.45-μm PTFE filters (Millipore). The concentration of TMA and its degradation products was analyzed by a Dionex ion chromatograph (IC, DX-120) equipped with a conductivity detector.

Effect of TiO_2 loading on RH-MCM-41 was studied by varying the amount of TiO_2 from 10 to 60 wt.%. The composite catalyst concentration was also varied from 0.25 to 2.0 g/L to optimize the reaction condition. The photocatalytic activities of bare TiO_2 and TiO_2/RH-MCM-41 were compared on the basis of the same loading of TiO_2. The effect of pH was studied in the range of 3–11. Furthermore, the catalytic activities of controlled reactions in the dark and under UV irradiation were compared. The mineralization of TMA was also analyzed by monitoring the total organic carbon (TOC) with a TOC analyzer (Shimadzu TOC-V_{CSH}).

Adsorption of TMA (80–120 μM) on the catalyst with the highest PCD activity was measured in the aqueous slurry of catalyst powder (at 1 g/L). The slurry pH was adjusted by HNO_3 or LiOH standard solutions. The slurry was sonicated for 30 s and stirred in the dark for 30 min. The sample aliquots of 1 mL were collected, filtered through 0.45-μm PTFE filters to remove catalyst

particles and analyzed for TMA by a Dionex ion chromatograph (IC, DX-120) equipped with a Dionex IonPac CS 12A (4 mm × 250 mm) column and a conductivity detector. The eluent for TMA analysis was 10 mM methanesulfonic acid.

3. Results and discussion

3.1. Characterizations of bare TiO_2 and TiO_2/RH-MCM-41

There are two ways to prepare the hybrid photocatalysts consisting of TiO_2 and MCM-41. One is to substitute Ti atom into the silicic framework of MCM-41 (Ti-MCM-41) [20] and the other to deposit TiO_2 nanoparticles on the external or pore surface of MCM-41 (TiO_2/MCM-41) [11]. The former is to make a solid solution of Ti in MCM-41 and the TiO_2 phase cannot be detected by XRD. On the other hand, the later method is to make a coupled composite of two material phases and the separate X-ray diffraction peaks for each phase should be observed. This work involves the preparation, characterization and photocatalytic activity of TiO_2/MCM-41 (the latter case).

The XRD patterns of RH-MCM-41 and TiO_2/RH-MCM-41 at low angles are shown in Fig. 1A. Three MCM-41 characteristic peaks at 2.3°, 4.1° and 4.7°, could be observed clearly on the RH-MCM-41 but the peak intensities of the TiO_2-loaded samples decreased with increasing the loading. It seems that the presence of TiO_2 on MCM-41 support scatters out the diffracted X-ray intensity. However, the peak position of the (1 0 0) plane little changed with loading TiO_2, indicating that the nanoparticles are located only on the surface of RH-MCM-41 and did not disrupt the pore structure. Similar intensity decrease was also observed in TiO_2/Al-MCM-41 prepared by solid state dispersion with loading 3–10 wt.% of TiO_2 [11]. The XRD patterns at higher angles of TiO_2/RH-MCM-41 and TiO_2 (P25) are shown in Fig. 1B. The bare TiO_2 which was used as-received composed of anatase and rutile phases with 80:20 ratio and both phases were confirmed by XRD. The intensities of TiO_2 on RH-MCM-41 increased with loading and that the phase ratio was maintained similar in all TiO_2/RH-MCM-41 samples. Similar results were observed when TiO_2 particles were loaded on SBA-15 [21].

The nitrogen adsorption–desorption isotherms of RH-MCM-41, TiO_2/RH-MCM-41 and bare TiO_2 are shown in Fig. 2A. The isotherms of RH-MCM-41 and TiO_2/RH-MCM-41 corresponded to type IV which is a typical isotherm of mesoporous materials. The volume adsorbed at low relative pressure (<0.1) decreased with increasing TiO_2 loading, which indicated the reduction of surface area. The specific surface areas and pore diameters of all catalysts are listed in Table 1. The specific surface area of TiO_2/RH-MCM-41 decreased with the loading of TiO_2 because the mass fraction of the porous support (MCM-41) is reduced with TiO_2 loaded. However, the reduction of the surface area cannot be explained only in terms of the dilution effect. When 10% TiO_2 was loaded on RH-MCM-41, the total surface area of TiO_2/RH-MCM-41 was reduced by about

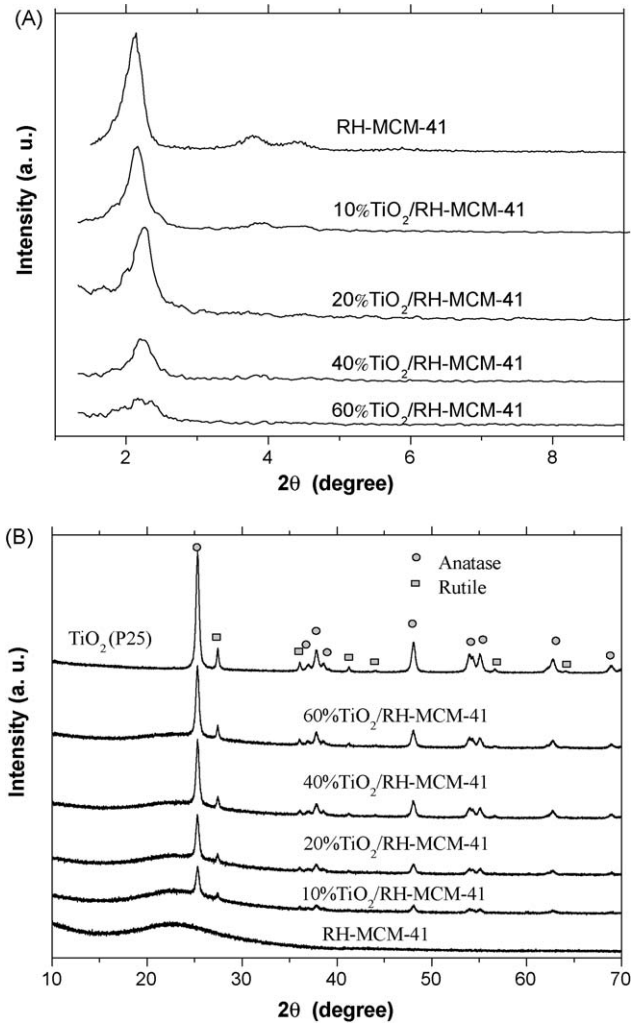

Fig. 1. XRD spectra: (A) low-angle XRD spectrum of RH-MCM-41 and TiO_2/RH-MCM-41 and (B) characteristic peaks of anatase and rutile phase of TiO_2 in bare TiO_2 and TiO_2/RH-MCM-41.

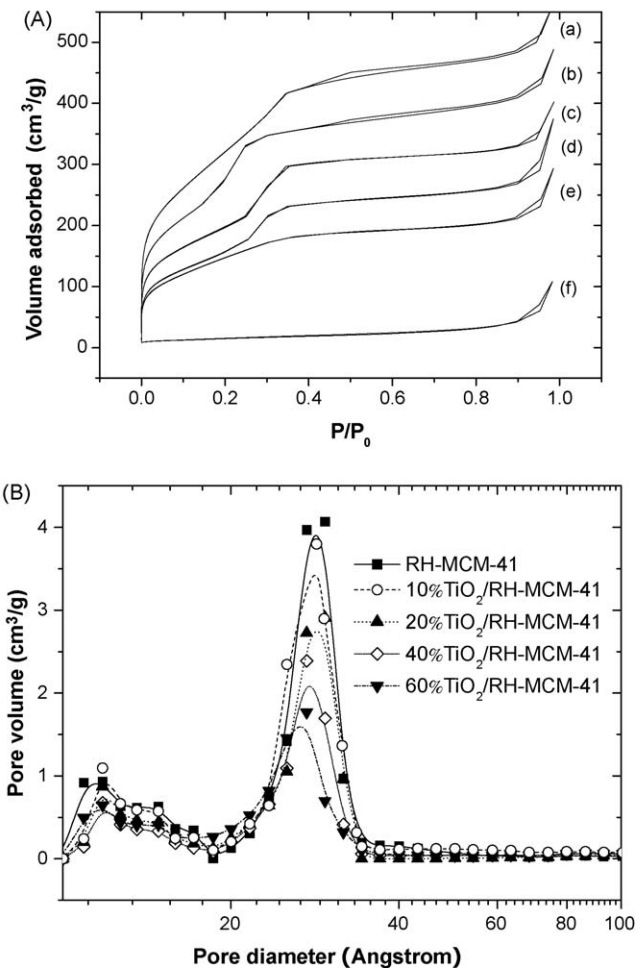

Fig. 2. (A) N_2 adsorption–desorption isotherm: (a) RH-MCM-41, (b) 10%TiO_2/RH-MCM-41, (c) 20%TiO_2/RH-MCM-41, (d) 40%TiO_2/RH-MCM-41, (e) 60%TiO_2/RH-MCM-41 and (f) bare TiO_2. (B) Pore size distribution in RH-MCM-41 and TiO_2/RH-MCM-41.

Table 1
BET surface area and average mesopore diameters of TiO_2, RH-MCM-41 and TiO_2/RH-MCM-41 at STP.

Materials	S_{BET} (m^2/g)	Mean pore diameter (Å)	Crystallize size of TiO_2 (nm)[a]
TiO_2 (P25)	53 ± 0.4	–	32.3
RH-MCM-41	943 ± 30	28.59 ± 0.03	–
10% TiO_2/RH-MCM-41	760 ± 25	28.45 ± 0.03	37.1
20% TiO_2/RH-MCM-41	729 ± 6	28.31 ± 0.02	46.0
40% TiO_2/RH-MCM-41	623 ± 8	27.63 ± 0.02	63.3
60% TiO_2/RH-MCM-41	590 ± 6	26.68 ± 0.01	101.2

[a] Calculated from Scherrer's equation: $t = K\lambda/(B\cos\theta)$ where t is the averaged dimension of crystallites; K is the Scherrer constant assumed to be 0.9 in this work; λ is the X-ray wavelength; and B is the peak width at half height (in radians 2θ) located at 2θ.

20%. This also implies that some fraction of the outer pore openings are blocked by the TiO_2 nanoparticles loaded on MCM-41 support [22]. The adsorbed volumes between relative pressure of 0.2 and 0.4 also decreased with increasing the amount of TiO_2 loaded. The hysteresis loop indicative of the mesoporous structure was outstanding with RH-MCM-41 and 10%TiO_2/RH-MCM-41 but vanished with the loading >20% TiO_2 which indicates that MCM-41 pore openings were blocked by the loaded TiO_2. Because the TiO_2 particle sizes are much larger than the size of mesopores, a partial clogging of outer pores in MCM-41 should be expected upon loading TiO_2 with the decrease of the available inner surface area, which was confirmed from the surface area measurement (Table 1). The pore diameters of all TiO_2/RH-MCM-41 calculated from BJH equation [23] were in the same range of 30–40 Å as shown in Fig. 2B. The typical pore size distribution of 10%TiO_2/RH-MCM-41 was comparable to the parent RH-MCM-41. Because the pore distribution profiles were largely unaffected by TiO_2 loading, the introduction of titania in the hybrid material did not destruct the pore framework of RH-MCM-41. The dispersion of TiO_2 nanoparticles on RH-MCM-41 support should prevent their agglomeration by maintaining the photocatalytic activity.

The TEM morphologies of RH-MCM-41, bare TiO_2 and 10%TiO_2/RH-MCM-41 are displayed in Fig. 3. The micrograph of RH-MCM-41 in Fig. 3A confirmed the highly ordered hexagonal arrays and one-dimensional mesoporous parallel channels. Fig. 3B showed nanoparticles of the bare TiO_2 (P25) with particle sizes in the 15–30 nm range. The particle sizes of TiO_2 on RH-MCM-41 were similar to those of bare TiO_2. The image of TiO_2 nanoparticles dispersed on RH-MCM-41 support is clearly seen in the high-resolution TEM image (Fig. 3D). Fig. 4 compares the elemental EDX images of O, Si, and Ti spots within the 10%TiO_2/RH-MCM-41 particles corresponding to Fig. 3C. The distribution of Si and O atoms almost exactly overlaps whereas Ti atoms were clearly differentiated from the silica support. Both TEM and EDX images show that the TiO_2 nanoparticles were well dispersed on RH-MCM-41.

The UV absorption spectra of TiO_2, TiO_2/RH-MCM-41, and RH-MCM-41 are compared in Fig. 5. The band gap excitation of TiO_2 loaded on MCM-41 was unaffected by the presence of MCM-41 support: the diffuse reflectance spectra did not show any change from bare TiO_2 (except for the dilution effect) in the absorption edge. The MCM-41 support did not show any sign of UV absorption. The UV absorption by TiO_2 on MCM-41 was saturated at 40%

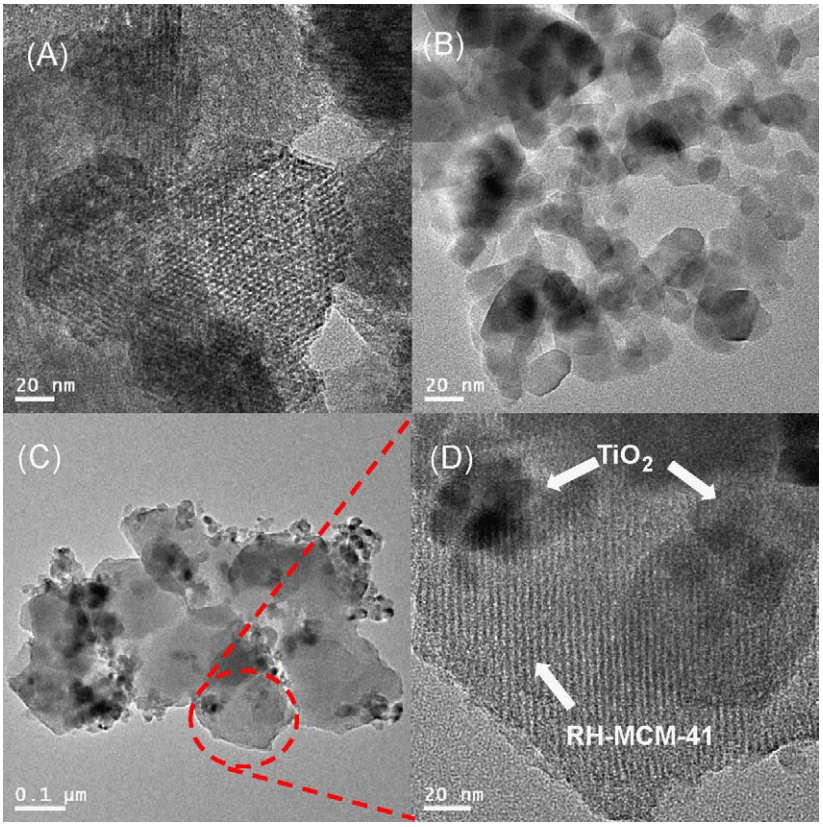

Fig. 3. High-resolution TEM images of RH-MCM-41, TiO_2 and 10%TiO_2/RH-MCM-41: (A) hexagonal structure of RH-MCM-41 (100k), (B) unsupported bare TiO_2 nanoparticles (25k), (C and D) TiO_2 particles on RH-MCM-41 (25k).

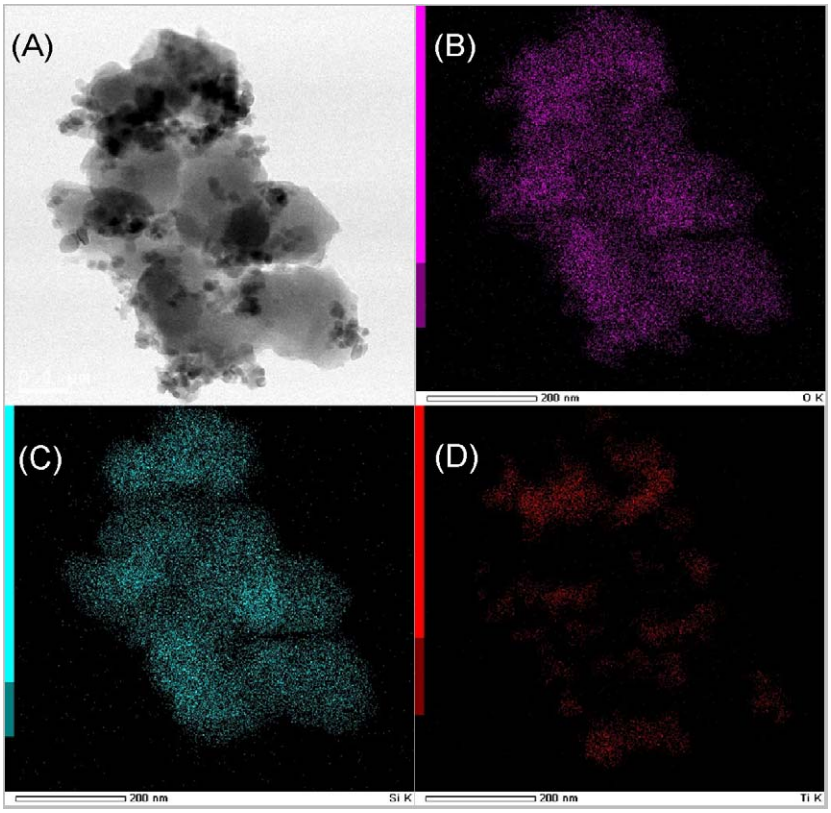

Fig. 4. Energy-dispersive X-ray images of (A) the scanning TEM bright field image and the elemental mapping of (B) O, (C) Si, and (D) Ti on 10%TiO_2/RH-MCM-41.

loading and the further increase to 60% did not induce any higher absorption of UV light. Since excessive loading of TiO_2 may result only in the aggregation and the reduction of the specific surface area (see Table 1), the optimal loading of TiO_2 on MCM-41 should be less than 40%.

Fig. 6 compares the pH-dependent zeta potential of RH-MCM-41, 10%TiO_2/RH-MCM-41, 40%TiO_2/RH-MCM-41, 60%TiO_2/RH-MCM-41 and bare TiO_2. The point of zero zeta potential (PZZP) increased in this order (pH 2.00, 2.90, 3.23, 4.10 and 6.08), which indicates that the surface charge of the hybrid catalyst is sensitively affected by the loading of TiO_2 [24,25]. Since TiO_2 is much less acidic ($pH_{zpc} \sim 6$) than MCM-41 ($pH_{zpc} \sim 2$), hybridizing TiO_2 with MCM-41 shifts the net surface charge to the negative side as shown in Fig. 6. Since the electrostatic attraction between TMA cations and the hybrid catalyst should be favored when the catalyst surface is negatively charged, the surface binding affinity for TMA should be higher with increasing the fraction of RH-MCM-41 component.

3.2. Photocatalytic degradation of TMA on bare TiO_2 and TiO_2/RH-MCM-41

The synergistic effect of combining TiO_2 and RH-MCM-41 is outstanding in Fig. 7A. The PCD of TMA was drastically enhanced with TiO_2/RH-MCM-41 while TiO_2 alone showed a minimal

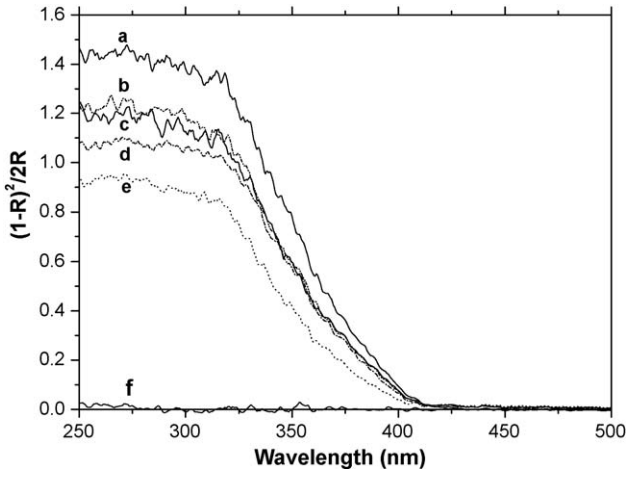

Fig. 5. UV–vis diffuse reflectance spectra of (a) TiO_2, (b) 60%TiO_2/RH-MCM-41, (c) 40%TiO_2/RH-MCM-41, (d) 20%TiO_2/RH-MCM-41, (e) 10%TiO_2/RH-MCM-41, and (f) RH-MCM-41 (the ordinate expressed in Kubelka–Munk unit; *R*, reflectance).

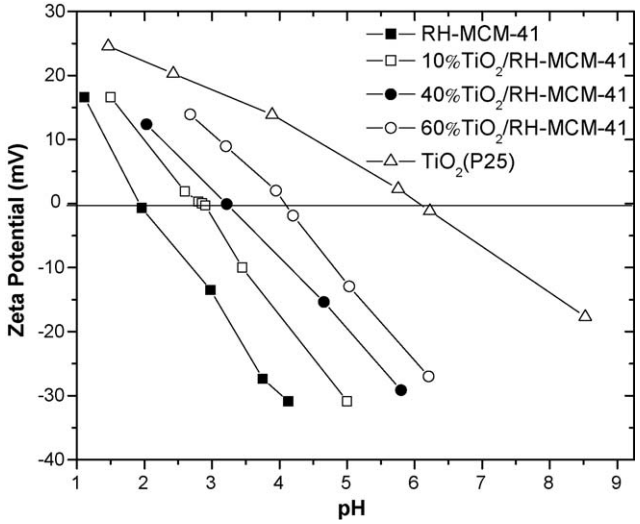

Fig. 6. Zeta potential of RH-MCM-41, TiO_2/RH-MCM-41 and TiO_2 suspended in water as a function of pH.

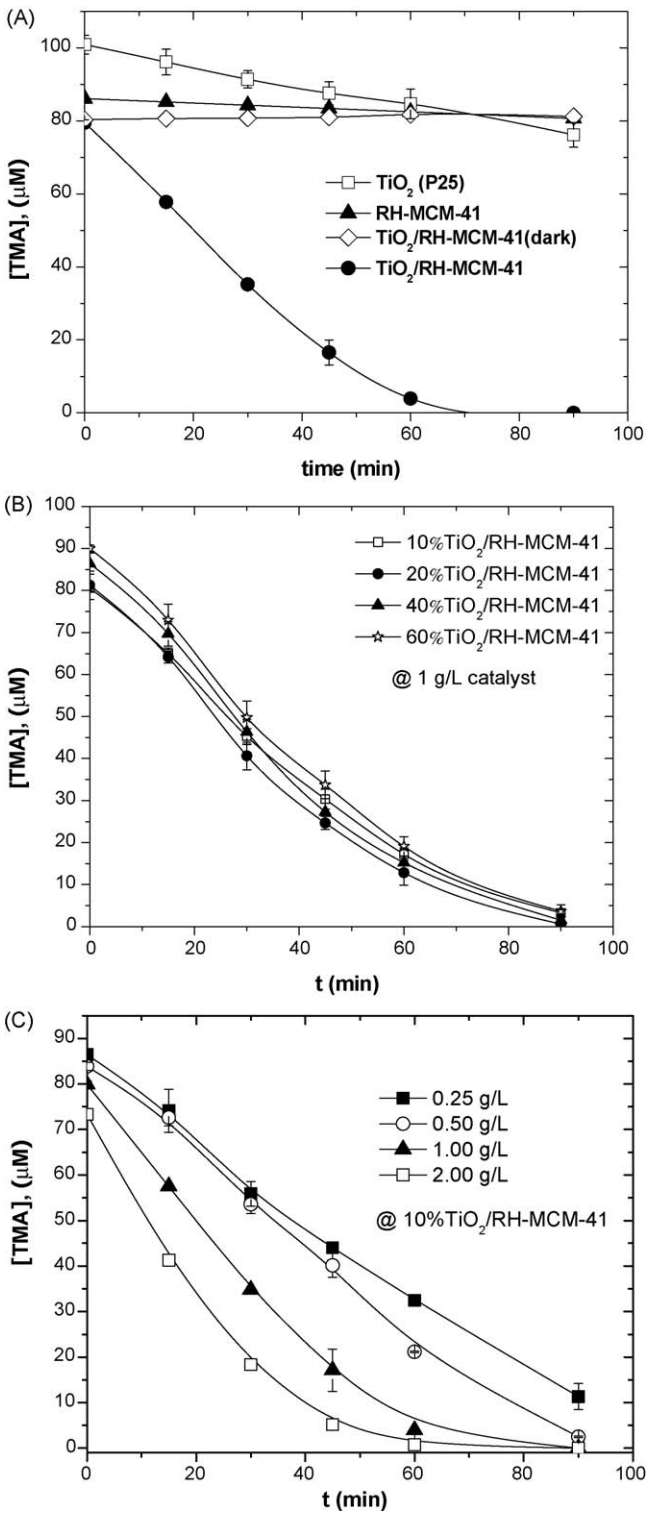

Fig. 7. (A) Photocatalytic degradation of TMA on TiO_2, RH-MCM-41 and 10%TiO_2/RH-MCM-41; [TiO_2] = 0.1 g/L, [RH-MCM-41] and [10%TiO_2/RH-MCM-41] = 1 g/L, pH 7. (B) Effect of TiO_2 content in TiO_2/RH-MCM-41 on the PCD rate of TMA; [TMA] = 100 μM, [cat] = 1 g/L, pH 7. The catalyst activity is compared on the basis of the total mass of the TiO_2/RH-MCM-41 (1 g/L).

activity at pH 7 and RH-MCM-41 alone was completely inactive. The effect of TiO_2 loading on RH-MCM-41 on PCD activity was also investigated. Fig. 7B shows that varying the TiO_2 loading (*i.e.*, 10, 20, 40 and 60 wt.%) has little effect on the PCD efficiency. 10%TiO_2/RH-MCM-41 was as good as 60%TiO_2/RH-MCM-41. That is, increasing the loading of TiO_2 over 10% on MCM-41 support did not increase the PCD activity. A recent work also reported that the 10 wt.% loading of TiO_2 was optimal in the TiO_2/Al-MCM-41 catalysts (in the range of 3–15 wt.%) when tested for the photocatalytic degradation of isoproturon [11]. On the other hand, when the total suspended mass of 10%TiO_2/RH-MCM-41 increased, the PCD activity did increase with the catalyst mass as Fig. 7C shows. That is Fig. 7B and C shows that increasing the total content of TiO_2 through different ways resulted in different responses. When the TiO_2 loading increased with the fixed mass of the hybrid catalyst, the loading over 10% did not enhance the PCD activity. However, when the total mass of the hybrid catalyst with 10% loading of TiO_2 increased, the PCD activity did. This observation indicates that the dispersiveness of TiO_2 on the support is critical in determining the PCD activity. The MCM-41 support overloaded with TiO_2 (>10%) does not show an enhanced activity despite the higher mass of TiO_2 probably because the direct interfacial contact between MCM-41 support and TiO_2 nanoparticles is lacking. Therefore, the synergic effect of combining TiO_2 particles and MCM-41 support is saturated at 10% loading and the higher loading is inefficient resulting in the separation between TiO_2 and MCM-41.

The marked synergism of the hybrid catalyst should be ascribed to the optimized surface charge and the dispersiveness of TiO_2 nanoparticles on the support. TiO_2 nanoparticles suspended around the neutral pH tend to be agglomerated because of the reduced surface charge density and hence the PCD activity for TMA was minimal near pH_{zpc} [1]. When TiO_2 particles are supported on MCM-41, the pH-induced agglomeration near pH_{zpc} can be minimized. In addition, MCM-41 can uptake a significant fraction of TMA in its pores through the electrostatic attraction (as Fig. 11 shows) and the adsorbed TMA can diffuse onto TiO_2 to undergo PCD. Alternatively, the OH radicals generated on TiO_2 surface can migrate to nearby TMA to initiate the degradation reaction [26]. In either case, the photocatalytic activity of the hybrid catalyst should increase due to the enhanced surface affinity for TMA.

The pH dependence of TMA PCD was compared between bare TiO_2 and 10%TiO_2/RH-MCM-41. Fig. 8 shows that the pH dependences are drastically different. The PCD activity of bare TiO_2 was minimal around pH 7 whereas that of 10%TiO_2/RH-MCM-41 was maximal around pH 7. The PCD activity of 10%TiO_2/RH-MCM-41 rapidly increased with raising pH from 3 to 7 since its

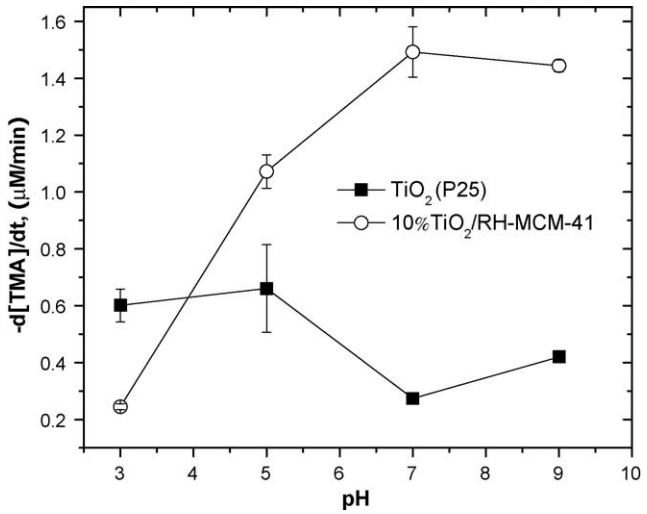

Fig. 8. Effect of pH on PCD of TMA in the suspension of bare TiO_2 and 10%TiO_2/RH-MCM-41; [TMA] = 100 μM, [TiO_2/RH-MCM-41] = 1 g/L, [TiO_2] = 0.1 g/L.

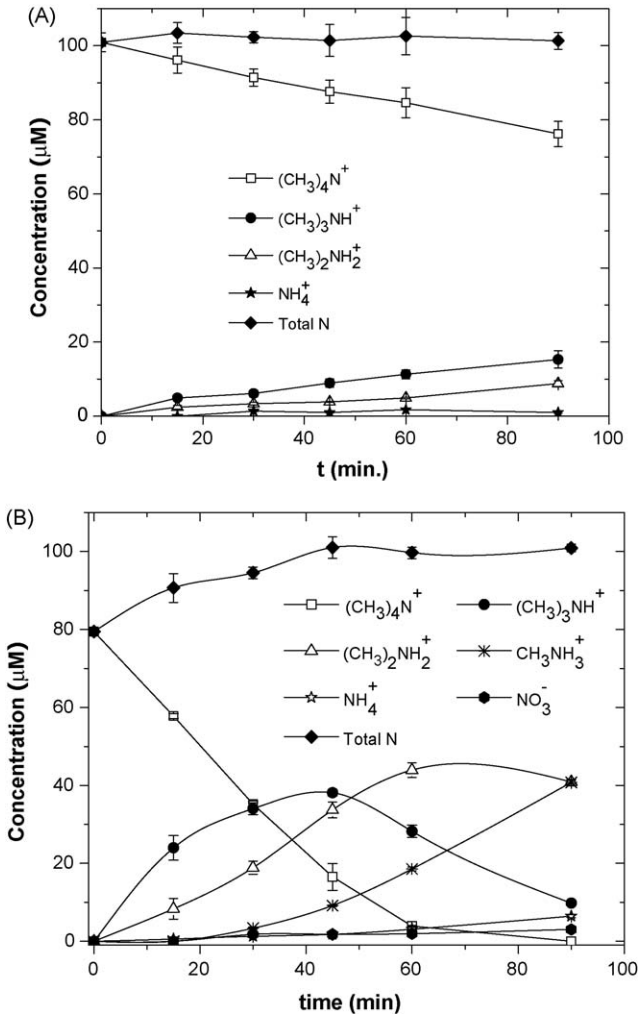

Fig. 9. Product distribution from the PCD of TMA: (A) bare TiO_2 and (B) 10%TiO_2/RH-MCM-41; [TMA] = 100 μM, [TiO_2/RH-MCM-41] = 1 g/L, [TiO_2] = 0.1 g/L, pH 7, $\lambda > 300$ nm.

surface charge becomes progressively negative in this pH region (see Fig. 6). On the other hand, the PCD activity of bare TiO_2 decreased in the same pH range because the surface charge approached zero when pH increased from 3 to 7. At pH 3, the zeta potential of 10%TiO_2/RH-MCM-41 is near zero (unstable slurry) while that of bare TiO_2 is positive (stable slurry). Although the surface affinity for TMA cations should be reduced with the positive surface charge, maintaining the dispersiveness of TiO_2 in the acidic condition seems to be more important than the TMA–surface interaction. Therefore, the PCD activity of 10%TiO_2/RH-MCM-41 is lower than bare TiO_2 at pH 3 but the activity order is reversed at pH $\geq$ 5. The PCD activity of 10%TiO_2/RH-MCM-41 was saturated above pH 7 while MCM-41 was not stable enough in the alkaline condition [27,28]. As a result, the PCD activity of 10%TiO_2/RH-MCM-41 was almost negligible at pH 11.

The products and intermediates generated during the PCD of TMA with bare TiO_2 and 10%TiO_2/RH-MCM-41 are compared in Fig. 9. In accordance with the previous study [1], the main degradation products were tri-, di-, and monomethylammonium along with trace amount of ammonium and nitrate. The PCD of TMA should proceed through the sequential demethylation that is initiated by the OH radical attack on the methyl group [1]. The first intermediate generated from the degradation of TMA should be trimethylammonium, which was confirmed in Fig. 9. Then, the generation of dimethylammonium and monomethylammonium was slowly followed. The total nitrogen balance was satisfactory throughout the irradiation time for both cases. Although TMA could be completely removed within 90 min irradiation with 10%TiO_2/RH-MCM-41, the complete mineralization should need much longer time. Fig. 10 compares the removal of TOC between bare TiO_2 and 10%TiO_2/RH-MCM-41 systems at various pH. Above pH 3, the hybrid catalyst is far better than bare TiO_2 in the mineralization efficiency. Figs. 9 and 10 clearly demonstrate that combining TiO_2 and MCM-41 not only increases the removal efficiency of the parent substrate (TMA) but also enhances its mineralization efficiency under UV irradiation.

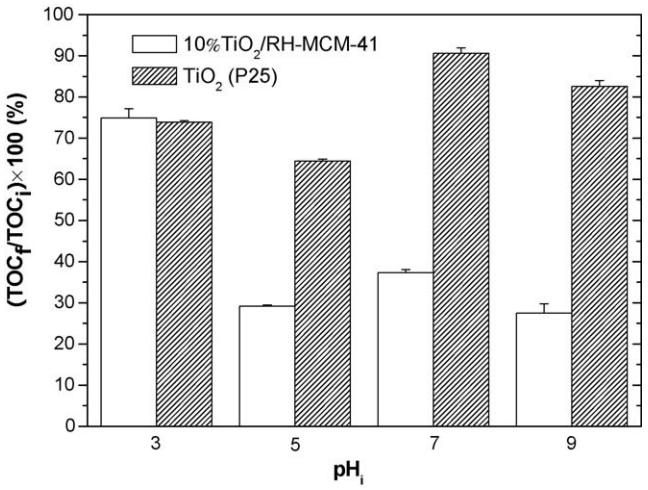

Fig. 10. TOC removal from PCD of TMA; [TMA] = 100 μM, pH 7, [10%TiO_2/RH-MCM-41] = 1 g/L, [TiO_2] = 0.1 g/L, $\lambda > 300$ nm, irradiation time = 90 min.

3.3. Adsorption of TMA on bare TiO_2 and 10%TiO_2/RH-MCM-41

The adsorption of TMA in the dark was investigated in the aqueous slurry of catalysts. After the equilibrium adsorption was established in 30 min, the amount of adsorbed TMA was measured and shown in Fig. 11A. The 10%TiO_2/RH-MCM-41 shows a much higher affinity for TMA adsorption compared with bare TiO_2. The TMA adsorption on TiO_2/RH-MCM-41 linearly increased with increasing the catalyst concentration from 0.25 to 2.0 g/L. On the other hand, the adsorption of TMA on bare TiO_2 was insignificant as reported previously [9] and showed little change with increasing the TiO_2 concentration. Such a highly enhanced adsorption of TMA on TiO_2/RH-MCM-41 should be mainly ascribed to the modification of the catalyst surface charge [29]. As shown in Fig. 6, the zeta potential (or surface charge) of 10%TiO_2/RH-MCM-41 was drastically shifted to the negative direction from that of bare TiO_2 (close to zero at pH 7) and this should highly favor the adsorption of TMA cations. The adsorption of TMA on 10%TiO_2/RH-MCM-41 exhibited a good Langmuirian behavior following Eq. (1) as shown in Fig. 11B.

$$\frac{C_e}{q_e} = \frac{C_e}{q_{\max}} + \frac{1}{K_{ad} q_{\max}} \quad (1)$$

C_e = equilibrium concentration of TMA in solution (mg/L); q_e = amount of adsorbed TMA on the catalyst at equilibrium (mg/g); $q_{\max}$ = maximum adsorption amount of TMA (mg/g); K_{ad} = Langmuir adsorption constant $(mg/L)^{-1}$.

The values of $q_{\max}$ and K_{ad} with 10%TiO_2/RH-MCM-41 were determined to be 8.34 mg/g and 2.90×10^{-2} $(mg/L)^{-1}$, respectively.

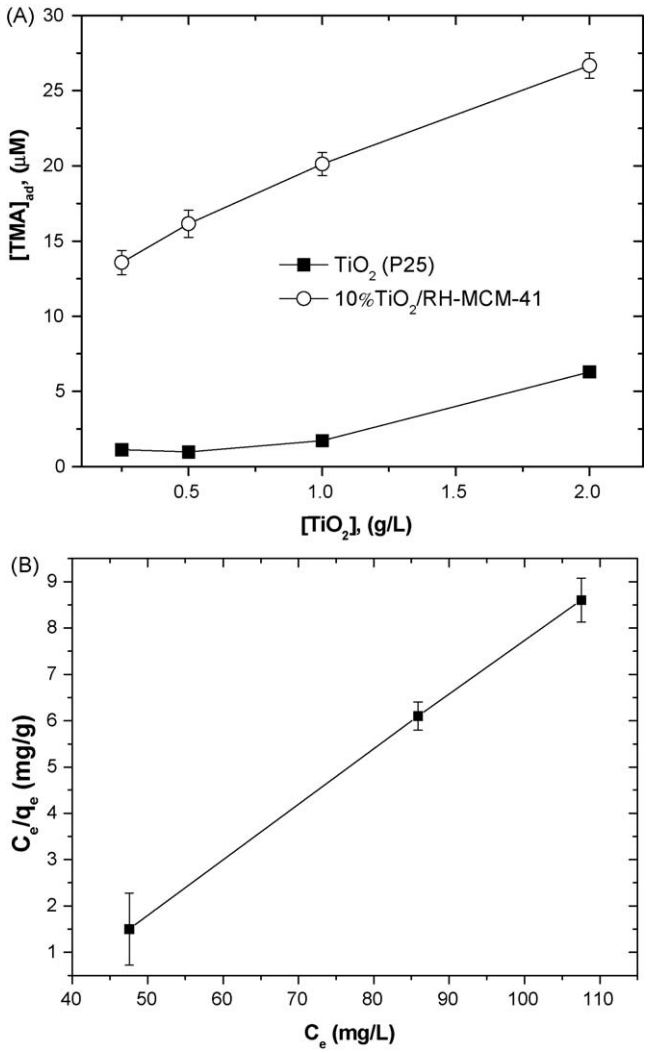

Fig. 11. (A) Adsorption of TMA on TiO_2 and 10%TiO_2/RH-MCM-41 in the aqueous slurry of catalyst in the dark: $[TMA]_0 = 100$ μM, pH 7. (B) Linearized plot of Langmuir isotherm of TMA adsorption on 10%TiO_2/RH-MCM-41: [TiO_2/RH-MCM-41] = 1 g/L, pH 7.

4. Conclusions

The photocatalytic degradation of TMA on TiO_2 nanoparticles could be highly enhanced by dispersing them on the support of RH-MCM-41. The dispersion caused a decrease in the support surface area due to partial pore blocking but the morphology, crystallinity and band gap energy of TiO_2 did not change. The TMA adsorption on TiO_2/RH-MCM-41 was much higher than that on the bare TiO_2 and was successfully described by the Langmuir model. A significant improvement in the photocatalytic activity was obtained with the hybrid catalyst and the optimal TiO_2 loading was 10 wt.%. The increase in the mass of hybrid catalyst (with a fixed % TiO_2 loading) caused a significant improvement in the photocatalytic activity whereas the increase in % TiO_2 loading on the support (with a fixed mass of the hybrid catalyst) did not enhance the PCD activity. The PCD activity of 10%TiO_2/RH-MCM-41 strongly depended on the solution pH and was maximal around the neutral pH while that of bare TiO_2 photocatalyst showed the reverse dependence on pH. A complete photocatalytic conversion of TMA was achieved in 90 min irradiation. Tri-, di- and monomethylammonium were generated as the main intermediates along with ammonium and nitrate as minor products. PCD with TiO_2/RH-MCM-41 was much faster not only for the removal of the parent substrate (TMA) but also its mineralization.

Acknowledgements

A scholarship for S. Artkla and research funding are from Synchrotron Light Research Institute (Public Organization) Grant 2-2548/PS01 and Suranaree University of Technology. W. Choi appreciates the financial supports from KOSEF/MEST grant (No. R0A-2008-000-20068-0) and the KOSEF EPB center (Grant No. R11-2008-052-02002).

References

[1] S. Kim, W. Choi, Environ. Sci. Technol. 36 (2002) 2019–2025.
[2] A. Bhattacharyya, S. Kawi, M.B. Ray, Catal. Today 98 (2004) 431–439.
[3] G. Li, X.S. Zhao, M.B. Ray, Sep. Purif. Technol. 55 (2007) 91–97.
[4] I.K. Konstantinou, T.A. Albanis, Appl. Catal. B: Environ. 49 (2004) 1–14.
[5] Z. Zhang, C.-C. Wang, R. Zakaria, J.Y. Ying, J. Phys. Chem. B 102 (1998) 10871–10878.
[6] C. Wei, W. Lin, Z. Zainal, N.E. Williams, K. Zhu, A.P. Kruzic, R.L. Smith, K. Rajeshwar, Environ. Sci. Technol. 28 (1994) 934–938.
[7] G.R. Heltz, A.C. Nweke, Environ. Sci. Technol. 29 (1995) 1018–1022.
[8] O. Carp, C.L. Huisman, A. Reller, Prog. Solid State Chem. 32 (2004) 33–177.
[9] M.S. Vohra, J. Lee, W. Choi, J. Appl. Electrochem. 35 (2005) 757–763.
[10] N. Bouazza, M.A. Lillo-Ródenas, A. Linares-Solano, Appl. Catal. B: Environ. 77 (2008) 284–293.
[11] M.V. Phanikrishna Sharma, V. Durga Kumari, M. Subrahmanyam, Chemosphere 72 (2008) 644–651.
[12] N. Grisdanurak, S. Chiarakorn, J. Wittayakun, Korean J. Chem. Eng. 20 (2003) 950–955.
[13] S. Chiarakorn, T. Areerob, N. Grisdanurak, Sci. Technol. Adv. Mater. 8 (2007) 110–115.
[14] H. Nur, L.C. Guan, S. Endud, H. Hamdan, Mater. Lett. 58 (2004) 1971–1974.
[15] H. Nur, H. Hamid, S. Endud, H. Handan, Z. Ramli, Mater. Chem. Phys. 96 (2006) 337–342.
[16] N.E. Poh, H. Nur, M.N.M. Muhid, H. Hamdan, Catal. Today 114 (2006) 257–262.
[17] J. Chumee, N. Grisdanurak, A. Neramittagapong, J. Wittayakun, Sci. Technol. Adv. Mater. 10 (2009) 015006.
[18] J. Wittayakun, P. Khemthong, S. Prayoonpokarach, Korean J. Chem. Eng. 24 (2008) 861–864.
[19] S. Artkla, N. Grisdanurak, S. Neramittagapong, J. Wittayakun, Suranaree, J. Sci. Technol. 15 (2008) 133–138.
[20] W. Lin, H. Han, H. Frei, J. Phys. Chem. B 108 (2004) 18269–18273.
[21] M.V. Phanikrishna Sharma, V. Durga Kumari, M. Subrahmanyam, Chemosphere 73 (2008) 1562–1569.
[22] B. Sun, E.P. Reddy, P.G. Smirniotis, Appl. Catal. B: Environ. 57 (2005) 139–149.
[23] S. Brunauer, P.H. Emmett, E. Teller, J. Am. Chem. Soc. 60 (1938) 309–319.
[24] Y.-L. Lin, T.-J. Wang, Y. Jin, Powder Technol. 123 (2002) 194–198.
[25] H. Chun, W. Yizhong, T. Hongxiao, Appl. Catal. B: Environ. 35 (2001) 95–105.
[26] W. Choi, S. Kim, S. Cho, H.-I. Yoo, M.-H. Kim, Korean J. Chem. Eng. 18 (2001) 898–902.
[27] P.C. Noda, E. Moreno, C.A. Henriques, S. Valange, Z. Gabelica, J.L.F. Monteiro, Micropor. Mesopor. Mater. 41 (2000) 137–148.
[28] L.Y. Chen, S. Jaenicke, G.K. Chuah, Micropor. Mater. 12 (1997) 323–330.
[29] H. Tada, Y. Kubo, M. Akazawa, S. Ito, Langmuir 14 (1998) 2936–2939.